A self-powered switching circuit for piezoelectric energy harvesting with velocity control

Y.-Y. Chen, D. Vasic, F. Costa, W.-J. Wu, C.-K. Lee

A self-powered switching circuit for piezoelectric energy harvesting with velocity control

Yu-Yin Chen[1,2], Dejan Vasic[1,3a], François Costa[1,4], Wen-Jong Wu[5], and Chih-Kung Lee[6]

[1] SATIE Lab (Systeme et Application des Technologies de l'Information et de l'Energie), UNIVERSud, ENS Cachan, France

[2] Institute of Applied Mechanics, National Taiwan University, Taiwan

[3] Université de Cergy-Pontoise, Neuville/Oise, France

[4] IUFM de Créteil, Université Paris 12, St Denis, France

[5] Department of Engineering Science and Ocean Engineering, National Taiwan University, Taipei, Taiwan

[6] Industrial Technology Research Institute of Taiwan, Taiwan

Received: date / Revised version: date

Abstract. The rapid development of low power consumption electronics and the possibility of harvesting energy from environmental sources can make totally autonomous wireless devices. Using piezoelectric materials to convert the mechanical energy into electrical energy for batteries of wireless devices in order to extend the lifetime is the focus in many researches in the recent years. It is important and efficient to improve the energy harvesting by designing an optimal interface between piezoelectric device and the load. In this paper, a self-powered piezoelectric energy harvesting device is proposed based on the velocity control synchronized switching technique (V-SSHI). Comparing to the standard full bridge rectifier technique, the synchronized switching harvesting on inductor (SSHI) technique can highly improve harvesting efficiency. However, in real applications when the energy harvesting device is associated with wireless sensor network (WSN), the SSHI technique needs to be implemented and requires being self-powered. The conventional technique to implement self-powered SSHI is to use bipolar transistors as voltage peak detector. In this paper, a new self-powered device is proposed, using velocity control to switch the MOSFET more accurately than in the conventional technique. The concept of design and the theoretical analysis are presented in detail. Experimental results are examined.

1 Introduction

Nowadays with improvement and rapid growth of low-power electronics, it is possible to supply portable devices such as mobile phone, MP3 player, wireless sensors and human or animal detecting devices, with harvest energy from ambient. Among these low-power devices, wireless sensor network (WSN) is one of the most important and valuable applications which is highly investigated. Wireless sensor networks can be used to monitor the health of structures, environment, wild animals, tire pressure of running cars, etc. In most of WSN applications, the devices are far from the power line or the devices need to be embedded into the structure to monitor. So, it is hard to use power line to transmit energy to device; battery is the only conventional solution. However, there are lots of disadvantages with using batteries. The major problem is the lifetime: using a 3 V battery a WSN can only be operated for 1 or 2 years. The batteries cannot be a permanent energy supply for WSN. A WSN with self-powered system can be operated for a longer time without replacing the battery. Harvesting the ambient energy close to the sensor nodes of the WSN is the most likely and suitable solution to extend the its lifetime [1-10]. There are various methods to convert mechanical ambient energy into electrical energy. According to the conversion mechanism, the power harvesting devices can be classified into three types: piezoelectric, electromagnetic and electrostatic [11]. Among these different types, piezoelectric transducers have been of great promise and interest.

The electric energy issued from a piezoelectric device is alternating voltage and current, so the simplest interfacing circuit that can be used is a standard DC approach (full bridge diodes rectifier). From studies [12], the efficiency of the standard DC approach is not optimal. There are lots of studies devoted to efforts to design and optimizing the interfacing circuits in order to improve the efficiency and maximizing the output power. A DC-DC converter is studied to match the impedance of the resistor load [9, 13]. The Synchronized Switch Harvesting on Inductor (SSHI) technique is a very successful and efficient technique to boost the output power from piezoelectrics [14-17]. This approach is derived from a semi-passive damping technique: Synchronized Switch Damping on Inductor (SSDI) [18-19]. The SSHI technique consists in adding up a nonlinear switching. This nonlinear process increases the output voltage of the piezoelectric elements that increase the output power. The switching device is triggered at the zero crossing of velocity. In order to realize the synchronized switching technique in real applications without external power source to supply the system, many researches present self-powered supply system for piezoelectric energy harvesting devices [4, 20-22]. The design concept of self-powered system proposed by [21] is shown in Figure 1. This conventional self-powered system works thank to a peak voltage detector to control the switching time for SSHI technique. However, the energy supplying the peak detector and the switching control is drawn from the piezoelectric device. The energy losses in the circuit

Send offprint requests to:

[a] *Present address:* vasic@satie.ens-cachan.fr

can be accurately controlled by circuit design; the larger excitation levels leading to relatively smaller losses. As the conventional self-powered system uses peak detector, there is always a phase lag between the peak voltage and the actual switching time. Moreover, the phase lag for large excitation level is less than for a small one [22].

In this paper, we present a new self-powered piezoelectric energy harvesting system using velocity control SSHI technique, called V-SSHI. The schematic design concept of self-powered velocity control SSHI is shown in Figure 2. The SSHI used herein is in series type (inductor and switch are in series with piezoelectric patch). Comparing to the conventional design concept, the piezoelectric material is separated into three parts. The main part is dedicated to harvest ambient vibration energy. The second small part is designed to supply energy for switching MOSFET and the last small part is designed for velocity control and for switching on the optimal time. There are two major advantages of this new technique: (1) theoretically, there isn't phase lag by using velocity control signal to determine the switching time; (2) the supply energy for the switching driver can be designed and optimized by the size of the piezoelectric material.

The energy flow chart of the conventional self-powered technique and the self-powered V-SSHI technique is shown in Figure 3. There is a common path for the main stream of energy and for the supply of the self-switching system. In the V-SSHI technique, they are three energy paths. The energy supplying the self-switching system and the velocity control patches can be designed optimally. The theoretical analysis and modeling of the standard DC and self-powered V-SSHI is presented in detail in section II. The experimental results comparing standard DC approach, conventional self-switched technique and V-SSHI technique are presented in section III. The experimental results show higher output power of the V-SSHI technique over conventional technique.

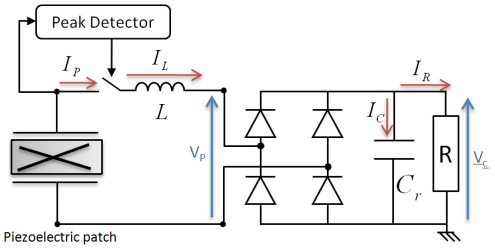

Fig. 1. Schematic design concept of conventional self-switched system

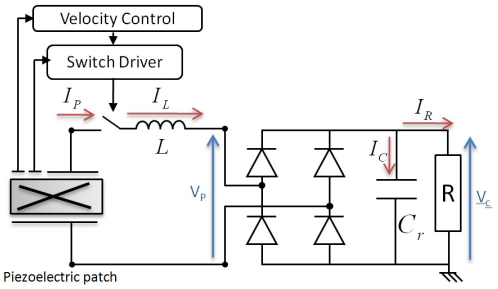

Fig. 2. Schematic design concept of velocity control SSHI self-switched system

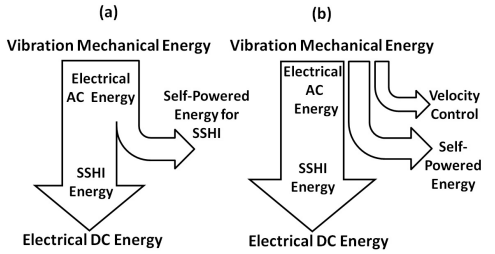

Fig. 3. Energy flow chart (a) Conventional self-powered technique (b) Self-powered V-SSHI technique

2 Theoretical analysis

The mechanical and electrical models of standard DC technique and V-SSHI technique are analyzed based on the following model. The analysis of piezo-element in this study is the same as for the classical model [17]. Considering the piezoelectric patches bounded on a cantilever beam, they can be regarded as a simple energy harvesting device. The dimensions of piezo-elements, schematic and coordinate directions are shown in Figure 4. When the cantilever vibrates, at the first mode, the force which acts on the piezoelectric patches can be simplified to a 1-D model and regarded as a force F acting on the lateral surface as shown in Figure 4. The piezoelectric equations (mechanical and electrical parts) can be expressed as follows (1):

$$\begin{aligned} F &= K_P^E x + \alpha V \\ I &= \alpha \dot{x} - C_0 V \end{aligned} \tag{1}$$

Where:

$$K_P^E = c_{11}^E \frac{w.t}{l} \tag{2}$$

$$\alpha = e_{31} w \tag{3}$$

$$C_0 = \varepsilon_{33}^S \frac{w.l}{t} \tag{4}$$

l, w, t denote length, width and thickness, and l, w are much larger than the thickness t. K_P^E is short-circuit stiffness, c_{11}^E is elastic constant in 1 direction, α is force-voltage coupling factor, e_{31} is piezoelectric constant, C_0 is clamped capacitance of piezoelectric and ε_{33}^S is permittivity constant.

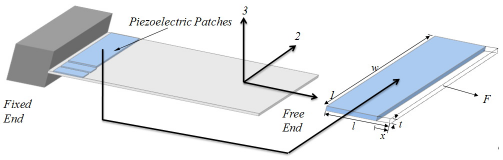

Fig. 4. Schematic of piezoelectric harvesting cantilever beam

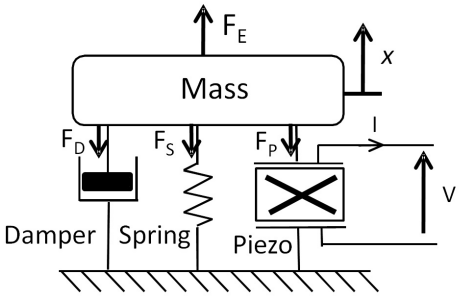

Fig. 5. Equivalent mechanical model of piezoelectric and structure

Table 1. Electrical and mechanical quantities

F_E	External driving force on the structure
F_D	Damping force from damper
F_S	Spring force from structure stiffness
F_P	Force from piezoelectric effect
x	Displacement
V	Voltage across the piezoelectric path
I	Current flow out from the piezoelectric path

An equivalent mechanical model including massproof, damper, spring and piezoelectric system as Figure 5 shows can model the piezoelectric cantilever beam, presented in Figure 4. The electrical and mechanical quantities are defined in table 1.

The governing equations of this model are expressed by (5):

$$\begin{aligned} m\ddot{x} + D\dot{x} + K^E x &= F_E - \alpha V \\ I &= \alpha \dot{x} - C_0 V \end{aligned} \tag{5}$$

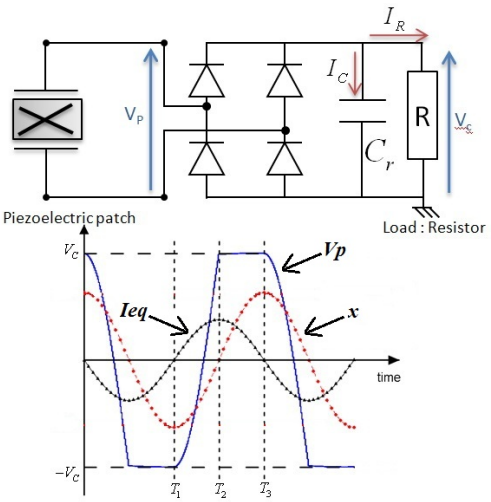

Fig. 6. The schematic diagram of the Standard DC approach and waveforms

D is the damping ratio of the structure, K^E is the equivalent stiffness of the structure and piezoelectric materials.

2.1 Standard DC technique

Before talking about the models of the V-SSHI technique, the standard DC technique is proposed to be a reference. The schematic diagram of piezoelectric energy harvesting transducer with full bridge rectifier connected to a resistor is shown in Figure 6. This is called standard DC technique. Assuming the structure is excited at the mechanical resonance frequency, the vibration velocity can be modeled by a current source, noted I_{eq}. Figure 6 shows also the key waveforms of the standard DC approach. When the absolute voltage value of the piezoelectric patch V_P is less than voltage V_C, the diode bridge is in open-circuit. The diodes conduct and piezoelements charge the load only when V_P reaches load voltage V_C.

According to the relation between force F_E, displacement x and velocity $\dot{x}$ (5), the output voltage V_C can be a function of excitation force $\hat{F}_E$ as (6) shown. The output power in the standard DC approach can be calculated using simple equation V_C^2/R as equation (7) shows.

$$V_C = \frac{2\alpha R\hat{F}_E}{(2RC_0\omega_0+\pi)D} \tag{6}$$

$$\begin{aligned} P &= \frac{V_C^2}{R} \\ &= \frac{4\alpha^2 R\hat{F}_E^2}{(2RC_0\omega_0+\pi)^2D^2} \end{aligned} \tag{7}$$

2.2 Self-powered V-SSHI technique

According to the self-powered V-SSHI concept presented in Figure 2, the model can be easily separated into three parts. The details are presented hereunder.

Main patch for SSHI

The main patch concerned with our new concept is designed to act like a classic SSHI technique. The schematic diagram of a SSHI technique is shown in Figure 7. The fundamental concept of SSHI is to use an inductor L and achieving a LC_0 resonance between piezo-element and L. Through LC_0 resonance and switches to confine the current flow, more power can be harvested from the piezo-element. Assuming the structure is excited at the mechanical resonance frequency, the excitation source can be modeled as a current source I_{eq}. Figure 8 shows the waveform of SSHI-series including voltage across piezoelectric V_P, current source I_{eq} and displacement x.

Current I_R which flows through R from time period T_1 to T_3 is equal to the resonant current I_L. Considering the

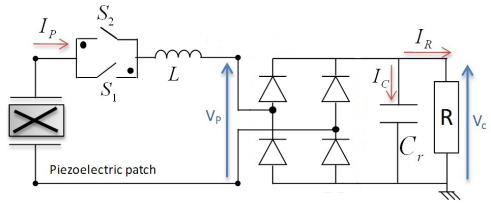

Fig. 7. Schematic diagram of SSHI piezoelectric energy harvesting device with full bridge rectifier to a resistor load

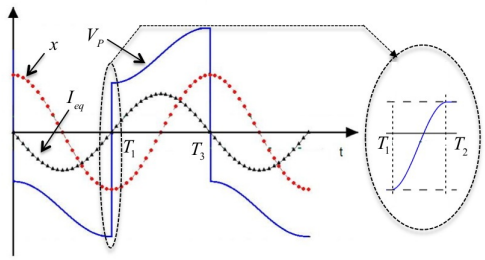

Fig. 8. Waveform of the SSHI piezoelectric energy harvesting device

time period from T_1 to T_3 and integrating I_R, the expression of the output voltage V_C can be obtained by (8). The output power from the transducer can be calculated using the simple formula V_C^2/R as shown in equation (9).

$$V_C = \frac{2\alpha R(1+\exp(\frac{-\pi}{2Q_I}))\hat{F}_E}{(2RC_0\omega_0(1+\exp(\frac{-\pi}{2Q_I})+\pi(1-\exp(\frac{-\pi}{2Q_I}))D} \tag{8}$$

$$\begin{aligned} P &= \frac{V_C^2}{R} \\ &= \frac{4\alpha^2 R(1+\exp(\frac{-\pi}{2Q_I})^2\hat{F}_E^2}{(2RC_0\omega_0(1+\exp(\frac{-\pi}{2Q_I})+\pi(1-\exp(\frac{-\pi}{2Q_I})))^2D^2} \end{aligned} \tag{9}$$

Considering the derivate of equation (9) relative to load resistance R, the optimal value R_{opt} of R can be calculated, it is expressed by (10).

$$R_{opt} = \frac{\pi(1-\exp(\frac{-\pi}{2Q_I}))}{2C_0\omega_0(1+\exp(\frac{-\pi}{2Q_I}))} \tag{10}$$

Substituting (10) into (9), the maximum power value P_{max} can be obtained, it is expressed by (11).

$$P_{max} = \frac{\alpha^2(1+\exp(\frac{-\pi}{2Q_I})\hat{F}_E^2}{2\pi C_0\omega_0(1-\exp(\frac{-\pi}{2Q_I})D^2} \tag{11}$$

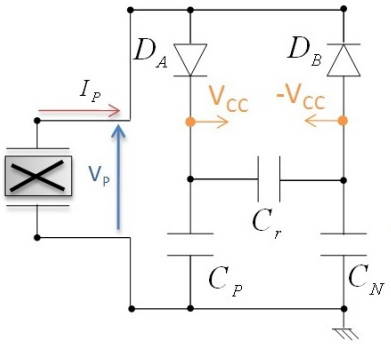

Fig. 9. The equivalent circuit diagram of the supplying circuit

Auxiliary patch for supplying the comparator

The second piezoelectric patch is designed to create two stable supply voltages $+V_{CC}$ and $-V_{CC}$ to supply energy to a comparator and make V-SSHI self-powered and self-switched. The velocity control input signal of the comparator is discussed in next part and the output signal of the comparator drives the two switches (NMOS and PMOS pair). The equivalent circuit of the supplying circuit is depicted in Figure 9. The two diodes D_A and D_B rectify the positive and negative current flow, C_R regulates the voltage between $+V_{CC}$ and $-V_{CC}$, C_P regulates the voltage between $+V_{CC}$ to GND and C_N regulates the voltage between $-V_{CC}$ to GND. Voltage V_{CC} can be obtained by integrating from T_1 to T_3 and the output power can be represented by V_{CC}^2/R_{eq} (13). Resistor R_{eq} is the equivalent load between $+V_{CC}$ and $-V_{CC}$.

$$V_{CC} = \frac{\alpha R_{eq}\hat{F}_E}{(C_0R_{eq}\omega_0+\pi)D} \tag{12}$$

$$\begin{aligned} P &= \frac{V_{CC}^2}{R_{eq}} \\ &= \frac{\alpha^2 R_{eq}\hat{F}_E^2}{(C_0R_{eq}\omega_0+\pi)^2D^2} \end{aligned} \tag{13}$$

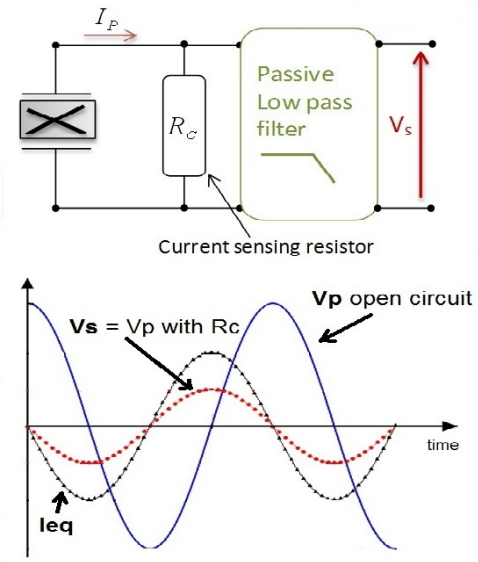

Fig. 10. The Equivalent circuit diagram of the velocity control circuit and the waveforms

Sensor patch for Velocity Control

The third patch is designed for generating the velocity control signal. The equivalent circuit is shown in Figure 10. A low value resistor R_C is connected in parallel with the patch to sense the mechanical current I_{eq}. A passive low-pass filter is used to reduce the high frequency noise. When SSHI works, the high frequency noise of the velocity signal is very large, so it is impossible to apply directly voltage V_P to comparator. The current sensing resistor used herein must be small enough to avoid the effect of the piezoelectric capacitance. The low-pass filter should be carefully designed to guarantee there is no phase lag for the considered frequency. The key waveforms are also shown in Figure 10. The blue line V_P is the open-circuit waveform of the piezoelectric patch and the red line V_S is the velocity control signal which is in phase with I_{eq}. There is 90 degree phase lag inherently between V_S and V_P. When the circuit switches by velocity control, the switching time can be accurate; the current is always in phase with voltage when SSHI works. The power output from piezoelectric can be always positive.

3 Experimental results and discussion

3.1 Experimental Setup

The experimental structure under test is a cantilever steel beam. Three 31-type PZT-QA piezoelectric ceramic patches provide by the company ELECERAM were bonded on the beam. Table 2 gives the dimensions of the beam and the patches. Figure 11 shows the experimental setup and the self-powered V-SSHI circuit diagram. Figure 12 shows a picture of the experimental setup. In the experimental setup, the SSHI circuit part is a little bit different from the one of Figure 7, but it works identically. The four diodes act like a full bridge rectifier to confine the current flow and the inductor is in series with P_1.

The cantilever beam is excited by a vibration shaker (LDS-V406). Three piezoelectric patches (P_1 to P_3) are bounded close to the fixed end. An accelerometer (PCB-353B03) is situated at the fixed end to measure acceleration; a laser vibrometer (LK-G32) measures the displacement at the free end. P_1 is the main patch for harvesting power. The circuit connected to P_1 for SSHI is composed of several parts: an inductor L for LC_0 resonance to enhance the power; four schottky diodes (D_1 to D_4) for confining the current flow; the load composed of a resistor and a capacitor; NMOS (2N7002) and PMOS (NDS0610) pair for

positive and negative switching. There are two stages for switching:

-when velocity crosses zero from negative to positive, voltage P_1 is at the maximal positive value, the NMOS is switched at this time and the SSHI process will occur through the path L-D_1-LOAD-D_3-NMOS.

-the negative stage works with the same logic through the path L-D_2-LOAD-D_4-PMOS.

Patch P_2 is connected to circuit composed of two schottky diodes and three capacitors to generate the positive voltages $+V_{CC}$ and $-V_{CC}$ for supplying comparator (TLV3701). Voltage V_{CC} should be larger than 2.5V to make sure that the comparator fully works to drive MOSFET. The comparator chosen here is a nano-power comparator from TI and the supplying current is only 560nA/per channel. This nano-power comparator is very easy to drive and suitable for low power circuit design. Patch P_3 is designed for velocity control. It is connected to a current sensing resistor followed by a passive low-pass filter. The resistor used herein is small enough to make sure there is no phase lag. The velocity signal noise (sine wave ideally) is attenuate by the low-pass filter. A comparator is used in order to generate the switching signal (square wave ideally) to drive NMOS and PMOS. The low-pass filter is designed to reduce high-frequency noise without phase lag. Figure 13 shows the experimental waveforms of the self-powered V-SSHI device.

Table 2. Dimension of the electromechanical transducer

Steel beam	
LengthxWidthxThickness	168.5mm x 94.3mm x 15mm
First bending mode	41.4Hz
Piezoelectric pathes (PZT-QA)	
P1	38.1mm x 16.5mm x 0.5mm
P2	15mm x 5mm x 0.5mm
P3	15mm x 5mm x 0.5mm

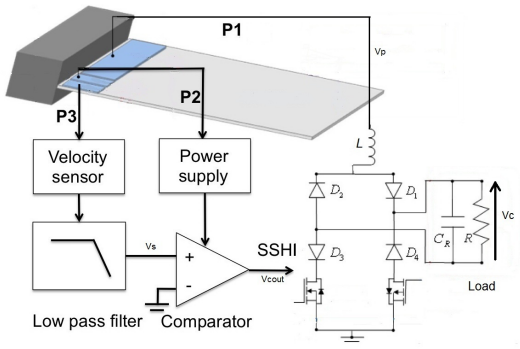

Fig. 11. Experimental setup and circuit diagram of V-SSHI device

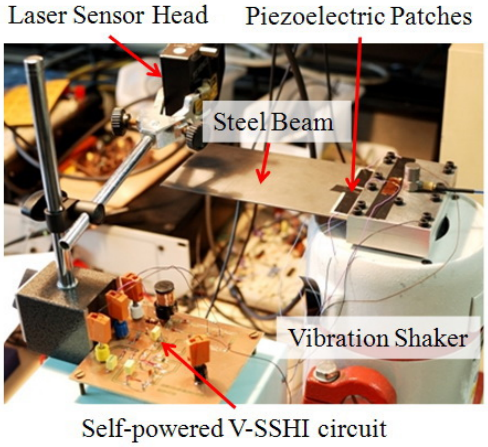

Fig. 12. Picture of the experimental setup and circuit

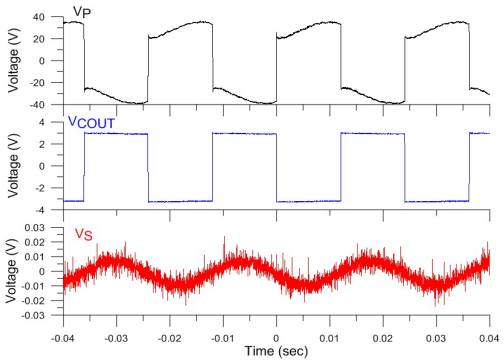

Fig. 13. Experimental waveform of the self-powered V-SSHI

3.2 Experimental results

Figure 13 shows three waveforms:

- black line V_P is the waveform of the piezoelectric patch P_1,

- blue line V_{Cout} is the output waveform of the comparator,

- red line V_S is the velocity control signal after the low-pass filter.

Although there is still some high frequency noise in the velocity control signal V_S, the comparator work still well; it is a tradeoff between reducing noise and phase lag. Observing waveform V_P, we can note that the switching time occurs almost at the peak value of the voltage.

The model parameters, identified by measurements, are given in table 3. The experimental and theoretical results of output power are shown in Figure 14. All experimental data are acquired for the same acceleration ($a = 2.5m/s^2$). The theoretical curves for standard DC and standard SSHI are drawn from equations (5), (7) and parameters in table 2. The standard DC experiment (measured using Figure 6 circuit) and "SSHI-Experiment" (measured by power supply and function generator using Figure 7 circuit) are the reference lines compared to theoretical lines; results show good agreement with predictions. Piezoelectric patch P_3 can be replaced by a smaller one. So, in the experiments of this study, the effect of patch P_3 is neglected. The experimental results (blue point) called "SSHI-Experiment" are measured on the conventional SSHI technique powered by external switching signal. The self-powered V-SSHI technique (red point) is measured by only one patch P_1. The output power of V-SSHI circuit is lower than the one of "SSHI-Experiment" circuit, because the energy is split to supply the auxiliary self-powered circuit. The conventional self-powered technique proposed by [22] is the line with green points. Experimental results show that the maximum output power of self-powered V-SSHI is higher than the conventional technique, essentially due to the efficient phase control.

Table 3. Measurements and model parameters

f_0	Short circuit resonance frequency	41.41Hz
f_1	Open circuit resonance frequency	41.45Hz
ξ	Open circuit damping coefficient	0.00105
C_0	Clamped capacitance P_1	25nF
C_0	Clamped capacitance P_2	3.5nF
C_0	Clamped capacitance P_3	3.5nF
α	Force-Voltage coupling factor	0.00069N/V
k^2	Electromechanical coupling factor	0.00193
M	Mass	182g
K^E	Equivalent stiffness of the source	12 320N/m
D	Damping of the structure	0.1N/m/s

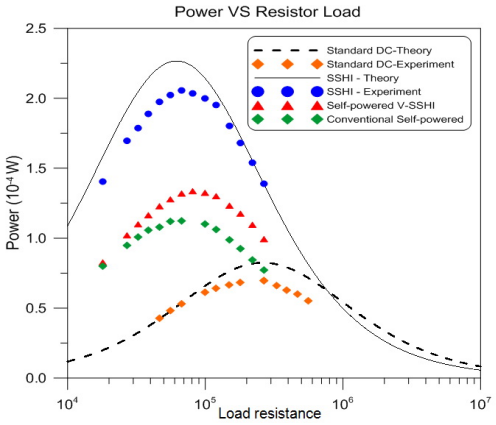

Fig. 14. Experimental Results

4 Conclusion

In this study, a self-powered V-SSHI piezoelectric energy harvesting is proposed, this is a new design concept. Based on the outstanding performance of SSHI technique, the self-powered V-SSHI circuit is fully self-powered, requiring no external power supply and though the velocity control, the switching time can be more accurate than with state-of-the-art techniques. The performance of the conventional self-powered circuit is close to the theoretical values of the SSHI; however, it requires an excitation level high enough to work properly [22]. In the self-powered V-SSHI technique, the excitation level doesnt influence the performance and when the supply voltage of the comparator is larger than 2.5V, the whole circuit fully works. The experimental results show better performance and lead to a gain of around 200% compared to the standard DC approach. Of course, the V-SSHI output power is lower than the theoretical SSHI, because the energy is split to supply the auxiliary self-powered circuit.

The architecture proposed in this study is more beneficial and represents a new step of the design concept. This circuit is easily used in real applications and may be combined with wireless sensor networks.

References

1. K. Yuse, T. Monnier, L. Petit, E. Lefeuvre, C. Richard, and D. Guyomar, Journal of Intelligent Material Systems and Structures, vol. 19, pp. 387-394, 2008.
2. C. O. Mathuna, T. O'Donnell, R. V. Martinez-Catala, J. Rohan, and B. O'Flynn, Talanta, vol. 75, pp. 613-623, May 2008
3. M. Lallart, D. Guyomar, Y. Jayet, L. Petit, E. Lefeuvre, T. Monnier, P. Guy, and C. Richard, Sensors and Actuators a-Physical, vol. 147, pp. 263-272, 2008.
4. D. Guyomar, Y. Jayet, L. Petit, E. Lefeuvre, T. Monnier, C. Richard, and M. Lallart, Sensors and Actuators a-Physical, vol. 138, pp. 151-160, 2007.
5. J. A. Paradiso and T. Starner, Pervasive Computing, IEEE, vol. 4, pp. 18-27, 2005.
6. S. Roundy and P. K. Wright, Smart Materials & Structures, vol. 13, pp. 1131-1142, Oct 2004.
7. S. Meninger, J. O. Mur-Miranda, R. Amirtharajah, A. Chandrakasan, and J. H. Lang, IEEE Transactions on, vol. 9, pp. 64-76, 2001.
8. R. Amirtharajah and A. P. Chandrakasan, IEEE Journal of, vol. 33, pp. 687-695, 1998.
9. G. K. Ottman, H. F. Hofmann, A. C. Bhatt, and G. A. Lesieutre, Power Electronics, IEEE Transactions on, vol. 17, pp. 669-676, 2002.

10. M. Ferrari, V. Ferrari, M. Guizzetti, and D. Marioli, Smart Materials & Structures, vol. 18, Aug 2009.

11. P. D. Mitcheson, T. C. Green, and E. M. Yeatman, Microsystem Technologies-Micro-and Nanosystems-Information Storage and Processing Systems, vol. 13, pp. 1629-1635, Jul 2007

12. E. Lefeuvre, A. Badel, A. Benayad, L. Lebrun, C. Richard, and D. Guyomar, Journal De Physique IV, vol. 128, pp. 177-186, 2005.

13. M. J. Guan and W. H. Liao, Smart Materials & Structures, vol. 16, pp. 498-505, 2007.

14. A. Badel, D. Guyomar, E. Lefeuvre, and C. Richard, Journal of Intelligent Material Systems and Structures, vol. 16, pp. 889-901, 2005.

15. D. Guyomar, A. Badel, E. Lefeuvre, and C. Richard, IEEE Transactions on Ultrasonics Ferroelectrics and Frequency Control, vol. 52, pp. 584-595, 2005.

16. E. Lefeuvre, A. Badel, C. Richard, and D. Guyomar, Journal of Intelligent Material Systems and Structures, vol. 16, pp. 865-876, 2005.

17. A. Badel, D. Guyomar, E. Lefeuvre, and C. Richard, Journal of Intelligent Material Systems and Structures, vol. 17, pp. 831-839, 2006.

18. C. Richard, D. Guyomar, D. Audigier, and G. Ching, Proc. SPIE: Smart Structures and Materials 1999: Passive Damping and Isolation vol. 3672, pp. 104-111, 1999.

19. C. Richard, D. Guyomar, D. Audigier, and H. Bassaler, Proc. SPIE: Smart Structures and Materials 2000: Damping and Isolation, vol. 3989, pp. 288-299, 2000.

20. T. H. Ng and W. H. Liao, Journal of Intelligent Material Systems and Structures, vol. 16, pp. 785-797, Oct 2005.

21. M. Lallart and D. Guyomar, Smart Materials & Structures, vol. 17, 2008.

22. L. Junrui and L. Wei-Hsin, in Information and Automation, 2009. ICIA '09. International Conference on, 2009, pp. 945-950.